Multiscale Approach to Ablation Modeling of Phenolic Impregnated Carbon Ablators

Jean Lachaud,* Ioana Cozmuta,† and Nagi N. Mansour‡
NASA Ames Research Center, Moffett Field, California 94035

A multiscale approach is used to model and analyze the ablation of porous materials. Models are developed for the oxidation of a carbon preform and of the char layer of two phenolic impregnated carbon ablators with the same chemical composition but with different structures. Oxygen diffusion through the pores of the materials and in depth oxidation and mass loss are first modeled at the microscopic scale. The microscopic model is then averaged to yield a set of partial differential equations describing the macroscopic behavior of the material. Microscopic and macroscopic approaches are applied with progressive degrees of complexity to gain a comprehensive understanding of the ablation process. Porous medium ablation is found to occur in a zone of the char layer that we call the ablation zone. The thickness of the ablation zone is a decreasing function of the Thiele number. The studied materials are shown to display different ablation behaviors, a fact not captured by current models that are based on chemical composition only. Applied to Stardust's phenolic impregnated carbon ablator, the models explain and reproduce the unexpected drop in density measured in the char layer during Stardust postflight analyses [Stackpoole, M., Sepka, S., Cozmuta, I., and Kontinos, D., "Post-Flight Evaluation of Stardust Sample Return Capsule Forebody Heat-Shield Material," AIAA Paper 2008-1202, Jan. 2008].

Nomenclature

C	=	oxygen concentration, $\mathrm{mol/m^3}$
D	=	diffusion coefficient, $\mathrm{m^2/s}$
D_{dis}	=	dispersion coefficient, $\mathrm{m^2/s}$
d_p	=	mean pore diameter, m
f	=	rarefaction function
J	=	molar ablation rate, $\mathrm{mol/m^2/s}$
Kn	=	Knudsen number
k	=	reactivity, m/s
L_D	=	diffusion length, m
L_R	=	reaction length, m
L_0	=	sample initial length, or thickness, m
M	=	molar mass, kg/mol
$\mathbf{n}$	=	vector normal to the surface
P	=	pressure, Pa
Pe	=	Péclet number
P_f	=	local fiber perimeter, m
q	=	local molar flux density, $\mathrm{mol/m^2/s}$
R	=	ideal gas constant, 8.314 J/mol/K
$S(x, y, z, t)$	=	surface function
S_p	=	local horizontal section of a pore, $\mathrm{m^2}$
s	=	volume surface, $\mathrm{m^2/m^3}$
T	=	temperature, K
V	=	averaging volume, $\mathrm{m^3}$
$\mathbf{v}$	=	velocity, m/s
$\bar{v}$	=	molecular agitation mean velocity, m/s
x, y, z, t	=	space (m) and time (s) coordinates
α	=	exponential coefficient for tortuosity law of the pore-filling matrix
γ_{ERSA}	=	effective reactive surface-area coefficient
ε	=	porosity
η	=	tortuosity
λ	=	mean free path, m
$\langle \xi_j^2 \rangle$	=	mean square displacement in direction j, m
ρ	=	density, $\mathrm{kg/m^3}$
Φ	=	Thiele number
Ω	=	solid molar volume, $\mathrm{m^3/mol}$

Subscripts

B	=	bulk
e, eff	=	effective
ERSA	=	effective reactive surface area
f	=	fiber
g	=	pyrolysis gases
i	=	indicator or index-number
K	=	Knudsen
m	=	matrix
ref	=	reference
w	=	wall

I. Introduction

A CRITICAL problem in the design of thermal protection systems (TPSs) for planetary probes and space vehicles is the choice of a heat-shield material and its associated material response model. The material response model is required to estimate the performance of the material for expected heat fluxes and load levels during atmospheric entry. An example of current generation of TPS material is PICA (phenolic impregnated carbon ablator) [1]. This material was used for Stardust and is a candidate for forthcoming NASA missions. The study in this paper aims to contribute to the analysis, modeling, and understanding of the behavior of PICA-like materials as a function of reentry conditions.
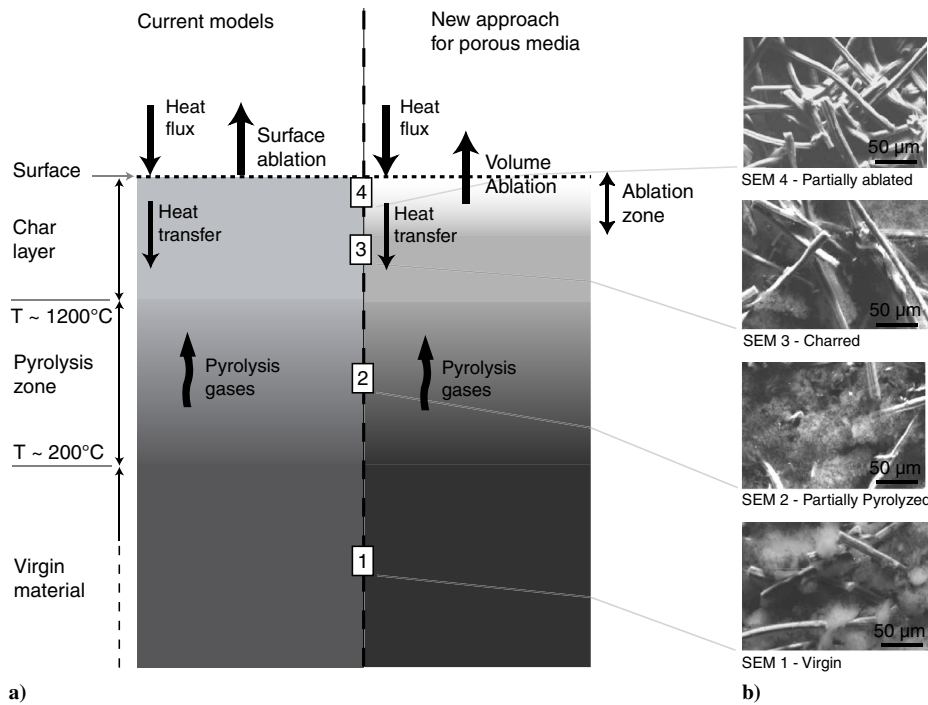
During reentry, part of the heat transfers inside the TPS (see Fig. 1a), leading to a gradual temperature increase of the material. As shown in Fig. 1b (SEM 1-virgin), PICA, in its virgin state, is made of a fibrous carbon preform consolidated by a pore-filling high-surface-area phenolic resin. With the temperature increase, the virgin material is successively transformed (and destroyed) by two phenomena [2]. The first transformation phenomenon is called pyrolysis. During pyrolysis, the phenolic resin is progressively carbonized into a low-density carbon, or charred (Fig. 1b, SEM 2-partially pyrolyzed) and

Fig. 1   Ablative material response to a reentry heat flux: a) simplified sketches of two possible models and b) postflight SEM micrographs of the Stardust TPS [4].

loses around 50% of its mass, producing pyrolysis gases (Fig. 1a). After pyrolysis, the material is a char composed of the fibrous carbon preform (unaffected by pyrolysis) and of the carbonized phenolic resin (Fig. 1b, SEM 3-charred). The second transformation phenomenon is called ablation (Fig. 1a). Depending on reentry conditions, ablation may be due to heterogeneous chemical reactions (oxidation and nitridation), phase change (sublimation), and/or mechanical erosion (spallation) of the char. These processes result in mass loss of the char and in a surface recession that are estimated using material response models.

Current material response models describe ablation as a surface phenomenon [2,3]; that is, all the mass is assumed to be lost at the surface, the material density being considered constant in the char layer. Current models repose on two major assumptions:

1) Ablation does not occur in volume (or this volume is negligible).

2) Equilibrium chemistry is considered in a control volume close to the wall [2].

In general, current models overestimate ablation rates because equilibrium chemistry is an upper-bound model (compared with possible finite rate chemistry). Stardust postflight analyzes have shown that the recessions on the flank and near the stagnation point, respectively, are overestimated by 20 and 61% using this description [4]. Finite rate chemistry models have been proposed and implemented to improve the accuracy of current models [5]. Ideally, heterogeneous finite rate chemistry models would require an estimation of the effective reactive surface area (ERSA) of the wall material. This is a complicated problem because the ERSA evolves with time and conditions. In the case of dense materials, the ERSA seems to be proportional to the surface roughness in practical applications [6]. In the case of porous materials, the ERSA is more likely a complex function of the porosity of the material and of the mass transport inside the pores [7]. A model predicting the ERSA is not available for PICA-like materials, but it would be needed for finite rate chemistry models considering surface ablation. This work contributes to the development of such models.

It is also important that the models correctly predict the evolution of the density profile of the TPS material. Stardust postflight analyzes have shown a correct overall agreement in the material density evolution between measurement and simulation using current models [4]. However, the models overpredict char-layer density close to the wall. The reason for this discrepancy could be that the

ablation of porous materials, such as PICA, cannot be accurately described as a surface recession (i.e., as a sharp ablation front propagation). This suggests that an ablation zone should be introduced to account for subsurface phenomena (Fig. 1a). Indeed, chemical reactions, phase changes, and even spallation (of the matrix) may occur in volume. Actually, in term of material modeling, addressing the modeling of the ablation zone is equivalent to developing ERSA prediction models. Multiscale approaches are required to provide phenomenological macroscopic models reflecting the material response at the microscopic scale. As a first step into this multiscale analysis, the focus is set on ablation by oxidation under Earth's atmospheric conditions (air).

From a microscopic-scale (fiber-scale) point of view, the matrix and fibers can differentially recess in depth when the conditions are such that oxygen molecules can penetrate the porous material and oxidation occurs in depth. An interpretation of the fact that the carbonized matrix is removed for the carbon preform shown in Fig. 1b (SEM 4-partially ablated) is that the recession due to oxidation is faster for the matrix than for the fibers. If this is a correct interpretation, ablation by oxidation is not a surface process for PICA-like materials, but is volumetric. As far as the material response is concerned, three important consequences follow this possible volume-ablation regime:

1) The ERSA of the material would be significantly increased.

2) The material would lose mass and weaken in volume, a condition that exposes the carbon fibers of the TPS material and may lead to spallation.

3) The ablation enthalpy distributed in volume would modify the thermal response of the material.

Hence, if the existence of an ablation zone is confirmed, a strong coupling of ablation and pyrolysis should be considered. In this context, the objective of this work is to anticipate when volume ablation may occur and to determine whether new pyrolysis-ablation models should be developed and used for TPS design with porous materials. We shall try to answer four questions:

1) What fraction of the oxygen that reacts on the wall in current models diffuses inside the porous medium and reacts in depth?

2) How deep is the reaction zone (in other words, what is the ERSA)?

3) What is the resulting char density distribution?

4) What is the depth of the resulting ablation zone?

The core of the article is organized in four sections. In Sec. II, a multiscale model for the oxidation of porous media is proposed. First, the microscopic-scale physics is modeled. The microscopic model would be computationally intensive for use at the engineering level (analysis and design). Therefore, a macroscopic model is derived from the microscopic equations using volume averaging. In Sec. III, both microscopic and macroscopic approaches are applied to the oxidation of a carbon preform. The objective of this section is to provide comprehensive understanding of the models. In Sec. IV, the models are applied to Stardust reentry conditions for two kinds of PICA-like materials. The two materials have the same chemical composition, density, and fiber preform architecture. However, the first material has a low-density pore-filling phenolic resin, and the matrix for the second material is a dense phenolic resin coating the fibers. The response of the two materials are compared (note that current ablation models would predict the same ablative behavior for these two materials, because they have the same chemical composition). Finally, we shall evaluate the ability of the macroscopic model to fit and explain the density profile measured on the Stardust TPS during postflight analyses.

II. Modeling Ablation by Oxidation of the Char Layer

We shall focus on ablation by oxidation of the char layer and assume that knowledge of the values of the intensive variables at the wall (pressure and temperature), the oxygen concentration at the wall, the thermal gradient in the material, and the velocity of pyrolysis gas blowing are necessary and sufficient to simulate the oxidation of the char layer. The oxidation model should be developed with knowledge of the order of magnitude of the physical parameters to capture the correct physics. These estimations are provided by current simulation tools. The aerothermal environment for the entry of Stardust was modeled [8] using the computational fluid dynamics (CFD) code Data Parallel Line Relaxation (DPLR) [9], assuming a ballistic entry and using the estimated flight trajectory (EFT) [10,11]. From the knowledge of the aerothermal environment, the material response for the Stardust EFT has been modeled [4] using the Fully Implicit Ablation and Thermal Analysis (FIAT) code [12].

In PICA, the matrix is an expanded high-surface-area phenolic resin that occupies the voids between the carbon fiber preform. In the virgin part of the material, the matrix protects the fibers against oxidation. In the char layer, however, the carbonized phenolic resin may be subject to oxidation, leaving the carbon fibers unprotected. The microscopic model then has to account locally for carbonized matrix and fiber ablation successively. This section is divided into two subsections. In Sec. II.A, the physics is first described and modeled at the microscopic scale, or fiber scale. In Sec. II.B, the microscopic model is spatially averaged to derive a macroscopic porous medium model.

A. Microscopic-Scale Model

The heterogeneous oxidation reaction in which carbon is consumed leads to carbonized matrix recession and reduction of fiber radius. The carbon fibers and matrix are assumed homogeneous and isotropic at the microscopic scale. The local motion of the material interface can be interpreted as a receding front with normal velocity proportional to the oxidation rate [6]. The interface is represented by a surface function $S(x, y, z, t)$ first-order differentiable almost everywhere, with constant value (zero) at the interface [13]. The function S satisfies the differential equation

$$\frac{\partial S}{\partial t} + \mathbf{v} \cdot \nabla S = 0 \tag{1}$$

where the recession velocity $\mathbf{v}$ is modeled as

$$\mathbf{v} = \Omega J \mathbf{n} \tag{2}$$

where Ω is the solid molar volume, J is the oxidation molar flux rate, and $\mathbf{n} = \nabla S / \|\nabla S\|$ is the unit normal pointing outward from the surface. For practical reasons, it may be convenient to use

several surface functions to describe distinct objects. For example, in the case represented in Fig. 2, a surface function per fiber was used.

We shall model carbon oxidation under air with a first-order heterogeneous reaction. For a first-order heterogeneous reaction, the local impinging molar flux density (on a fiber or carbonized matrix elementary surface) is given by

$$J = k_i C \tag{3}$$

where $C = C(x, y, z, t)$ is the oxygen concentration and k_i is, respectively, either fiber k_f or carbonized matrix k_m intrinsic reactivities. For Stardust entry trajectory at the wall stagnation point, DPLR simulations show that the ratio of atomic oxygen concentration to molecular oxygen concentration is lower that 20% when ablation becomes significant around 35 s after entry interface. After peak heating (51 s), the ratio is lower than 10%. Consequently, in the following, we shall neglect atomic oxygen and focus on oxidation by molecular oxygen. It is very difficult to accurately estimate the oxidation reactivity of carbonous materials, mainly because it is a strong function of all the details of the fabrication process. Using data from the studies cited in [5,14–16], fiber and carbonized matrix reactivities to molecular oxygen are estimated to be around

$$k_f = \frac{k_m}{10} = 100 \exp\left(-\frac{1.2 \times 10^5}{RT}\right) \tag{4}$$

where T is the local temperature and R is the ideal gas constant. The reactivity of the matrix is higher than the reactivity of the fibers because the pseudographitic structure of the carbonized phenolic matrix includes many more defects than carbon fibers [15].

The local concentration of oxygen is obtained by solving a mass balance equation featuring transport in the gas phase, from the wall and through the pores of the fibrous media. The determination of the location of the average solid/surrounding fluid interface (wall) is not obvious for rough or porous media. In a first approximation, we will keep the current model hypothesis and consider that the wall is defined by the surface delimited by the emerging fiber tips, as represented in Fig. 2.

In the phase of the reentry trajectory for which ablation is nonnegligible, the flow dynamics are in the continuum regime at the scale of the reentry body [8]. However, inside the porous medium, the length scale of interest is small and the dynamics may be in the rarefied gas regime. In porous media, the Knudsen number is defined as the ratio of the mean free path $\bar{\lambda}$ to the mean pore diameter d_p:

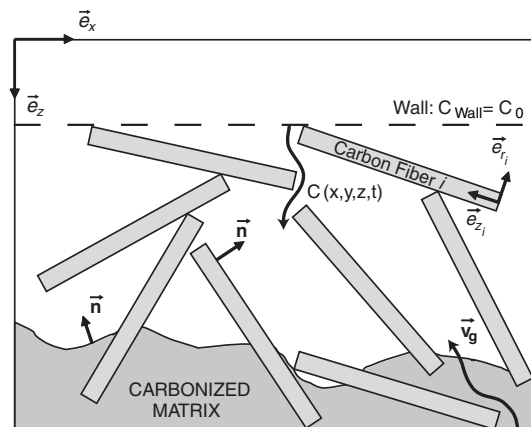$$Kn = \frac{\bar{\lambda}}{d_p} \tag{5}$$

Fig. 2 Sketch of the ablation zone of a PICA-like material at microscopic (fiber) scale.

For PICA-like materials, the mean pore diameter of the carbon preform is around 50 μm. The mean free path (in meters) of oxygen in air can be estimated using the following equation [17]:

$$\bar{\lambda} = 9.5 \times 10^{-8} \frac{10^5 T}{298 P} \qquad (6)$$

The different flow regimes in a porous medium with mean pore diameter $d_p = 50$ μm are shown in Fig. 3 as a function of pressure and temperature [using Eq. (6)]. The wall temperature-pressure values at the stagnation point along the Stardust trajectory are plotted in Fig. 3. This figure shows that mass transport at the pore scale has to be modeled using different methods, depending on the trajectory time. The Boltzmann equation is the fundamental mathematical model for gas flow at molecular scale [18]. For dilute gas dynamics (rarefied and transitional regimes), an efficient way to solve the Boltzmann equation is to follow a representative set of particles as they collide and move in physical space [19]. This integration method is called direct simulation Monte Carlo (DSMC) [18]. A Monte Carlo simulation tool that models mass transfer using random walks is presented and used in Sec. III.A. For gas dynamics in the continuum regime, the Navier–Stokes equations may be derived from the Boltzmann equation. This allows the use of analytical or CFD methods that are, in general, more efficient in the continuum regime than DSMC. In the slip regime, the continuum regime model may be used with allowance for discontinuities in velocity at solid boundaries [20].

Using the continuum mechanics formulation of fluid dynamics, the conservation of oxygen concentration in the fluid phase is given by [7]

$$\frac{\partial C}{\partial t} - \nabla \cdot (D \nabla C) + \nabla \cdot (C \mathbf{v}_g) = 0 \qquad (7)$$

where the second term models the binary diffusion of oxygen concentration in air according to Fick's law; D is the diffusion coefficient. The third term models the convective transport of oxygen concentration, where $\mathbf{v}_g$ is the local velocity of the fluid. The fluid velocity is driven by the pressure gradient arising from the production of pyrolysis gases. As a first cut, pyrolysis gases are assumed to be inert. They may actually react with the carbon preform (coking or oxidation) or with oxygen (homogeneous reactions).

For simple configurations, the system of Eqs. (1–3) and (7) can be solved analytically in steady state [6]. In the case of random fibrous media and/or Knudsen regime, direct numerical simulation (DNS) methods are required to find solutions on the microscale (see Secs. III.A and IV.A). Solutions at the microscopic scale are of interest for understanding and will be investigated in what follows. However, DNS has two main drawbacks:
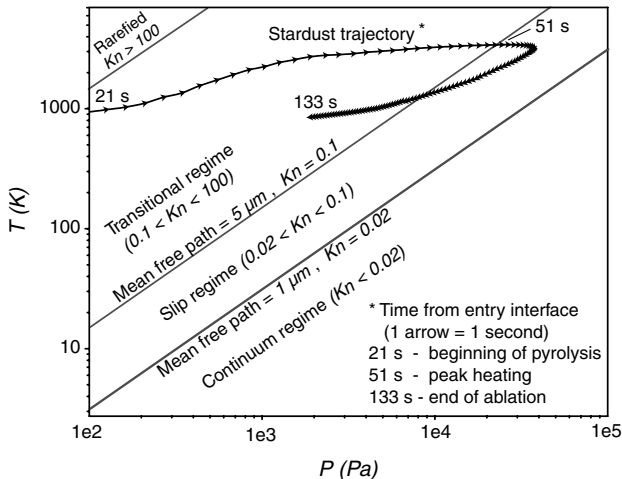
1) It is computationally intensive.

Fig. 3 Flow regimes encountered along Stardust reentry trajectory inside a porous medium of mean pore diameter 50 μm.

2) It can only address a limited part of the overall pyrolysis-ablation problem, because coupling with other phenomena, such as heat transfer or pyrolysis, would be difficult to handle at this scale.

A complementary approach consists of averaging the microscopic model to obtain equations at the macroscopic scale.

B. Macroscopic Model (Derived by Averaging the Microscopic Model)

The equations describing the material response at the microscopic scale are spatially averaged to derive equations describing the material response at the macroscopic scale of interest in the design of the TPS. This subsection is divided into two parts. In Sec. II.B.1, the equations describing the material evolution at the macroscopic scale are derived by averaging the local surface recession model [Eq. (1)]. In Sec. II.B.2, a closed form of the mass transport model in the porous medium is proposed.

1. Material Model

We will assume that the carbonized char layer is composed of three parts: the carbon perform, the carbonized matrix, and the void. The void ε (porosity), fiber ε_f, and matrix ε_m volume fractions are linked by the following relation:

$$\varepsilon + \varepsilon_f + \varepsilon_m = 1 \qquad (8)$$

It is of practical interest to build models for different material architectures to enable sensitivity analysis and possibly guide material design. We shall develop phenomenological models for three kinds of materials: 1) carbon preform without matrix, 2) carbon preform with carbonized matrix coating the fibers (Fig. 4a), and 3) carbon preform with carbonized matrix space filling (Fig. 4b). In this first multiscale approach that aims at providing some understanding, we chose to develop material models that are as simple and general as possible.

a. Model for Carbon Preform.

The preform of PICA-like materials will be modeled as a random array of carbon fibers. This material model is in qualitative agreement with the architecture of the preform shown in Fig. 1b (SEM 4). From the fabrication process of the fiber preform of PICA, we know that the fiber length is large compared with its diameter [1]. Therefore, fibers are going to ablate mainly due to radial recession, and recession in length can be neglected. At the initial time, each fiber i can be modeled as an infinite cylinder of circular section, with a time-dependent geometry that may be defined in cylindrical coordinates in the frame of the fiber axis $(\mathbf{e}_{r_i}, \mathbf{e}_{\theta_i}, \mathbf{e}_{z_i})$ (see Figs. 2 and 4). Assuming that the fiber section remains circular during the ablation process, one can remove the angular dependency, and the surface function may be written as $S_i(r_i, \theta_i, z_i, t) = r_i - r_f(z_i, t)$. The partial differential equation describing the evolution of the fiber radius $r_f(z_i, t)$ as a function of space and time is obtained by substituting this surface function in Eq. (1). After combining the expression for the fiber surface with Eqs. (2) and (3), we obtain

$$\frac{\partial r_f}{\partial t} = -\Omega_f k_f C \sqrt{1 + \left(\frac{\partial r_f}{\partial z_i} \right)^2} \qquad (9)$$
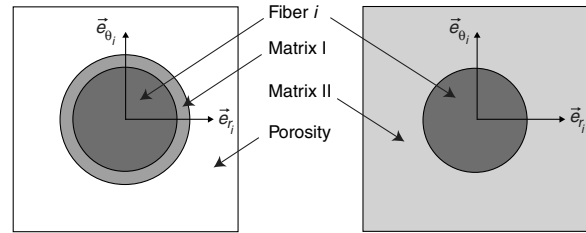
a) Matrix surrounding the fibers   b) Pore-filling matrix (assumed homogeneous at fiber scale)

Fig. 4 Two-dimensional sketches of the carbonized matrix models considered (the models are 3-D).

For an accurate analysis of the evolution of the fibers' geometry, this equation may be integrated [6], but this is not a simple task because C is a function of both space and time. In this first analysis of the ablation of random fibrous media, the point is not to accurately solve the evolution of the fibers' geometry but to gain an understanding of the overall behavior of the porous material. As a first cut, it is a reasonable approximation to neglect the evolution of the fiber radius as a function of z_i. Equation (9) can then be simplified to

$$\frac{\partial r_f}{\partial t} = -\Omega_f k_f C \qquad (10)$$

Using this equation, we could compute the recession of each fiber as a function of its location and of time, but this would yield more information than we need at the macroscopic scale. For design purposes, it is sufficient to determine the average fiber volume fraction associated with an averaging volume V: large compared with the fiber scales but small compared with gradients at the macroscopic scale. In the averaging volume, we shall assume that temperature and oxygen concentration are homogeneous. Under this hypothesis, k_f and C are only time-dependent variables in the averaging volume. The (average) fiber volume fraction can be expressed as a function of the time-dependent (average) fiber radius r_f:

$$\varepsilon_f = \varepsilon_{f,0} \left(\frac{r_f}{r_{f,0}}\right)^2 \qquad (11)$$

Subscript 0 indicates initial values. Combining Eqs. (10) and (11), we can derive a partial differential equation (PDE) directly describing the evolution of fiber volume fraction:

$$\frac{\partial \varepsilon_f}{\partial t} = -\frac{2\Omega_f k_f C}{r_{f,0}} \sqrt{\varepsilon_f \varepsilon_{f,0}} \qquad (12)$$

The specific surface for the fibrous medium treated as an arrangement of cylinders writes as

$$s_f = r_f \frac{2\varepsilon_{f,0}}{r_{f,0}^2} \qquad (13)$$

b. Model for Material I: Carbon Preform with Carbonized Matrix I.

The modeling of matrix oxidation depends on the matrix structure. For materials with a matrix surrounding the fibers (see Fig. 4a), one has to consider a cylinder of diameter $r_m = r_f + e_m$, where e_m is the thickness of the matrix layer. Matrix oxidation is modeled using

$$\frac{\partial r_m}{\partial t} = -\Omega_m k_m C \qquad (14)$$

where Ω_m is the molar volume of the matrix. Matrix volume fraction writes as

$$\varepsilon_m = \varepsilon_{m,0} \left(\frac{r_m^2 - r_{f,0}^2}{r_{m,0}^2 - r_{f,0}^2}\right) \qquad (15)$$

The specific surface is given by Eq. (13) using appropriate indices (m instead of f).

c. Model for Material II: Carbon Preform with Carbonized Matrix II.

This second model aims at modeling PICA using the simplest model possible. The carbonized matrix of PICA is a porous medium itself. However, its pore size is small compared with the mean free path. As a first approach, we will consider that oxygen cannot penetrate deeply inside the matrix without reacting. In other words, matrix II is assumed to be homogeneous at the scale of the fiber diameter, as represented in Fig. 4b. The matrix mass loss is proportional to its specific surface s_m and writes as

$$\frac{\partial \varepsilon_m}{\partial t} = -\Omega_m s_m k_m C \qquad (16)$$

In turn, s_m is a function of the volume fraction ε_m. This functional dependence is a strong function of the topology. Oxidation

experiments on the carbonized matrix will be needed to estimate this dependence. As a first cut, we assume the dependence to be linear.

2. Model for Oxygen Concentration

To solve Eqs. (10), (14), and (16), we could compute the local oxygen concentration everywhere in the porous medium. However, for design purposes, it is sufficient to determine the average oxygen concentration and the average rate of reaction associated with the averaging volume [7]. We decompose the local concentration in oxygen in the gas phase according to

$$C = \langle C \rangle^g + \tilde{C} \qquad (17)$$

where $\langle C \rangle^g$ is the intrinsic average concentration and $\tilde{C}$ is the spatial deviation concentration [7]. The intrinsic average concentration is defined by

$$\langle C \rangle^g = \frac{1}{V_g} \int_{V_g} C \, dV \qquad (18)$$

where V_g is the volume of the gas phase contained in the averaging volume V.

Accounting for a volume sink terms due to the heterogeneous consumption of oxygen, the mass balance equation in the porous medium closes as [7]

$$\varepsilon \frac{\partial \langle C \rangle^g}{\partial t} + \nabla \cdot \left(-(D_{\text{eff}} + D_{\text{dis}})\nabla \langle C \rangle^g \right) + \varepsilon f \langle \mathbf{v}_g \rangle^g \cdot \nabla \langle C \rangle^g$$
$$= -\langle C \rangle^g (\delta s_f k_f + s_m k_m) \qquad (19)$$

where D_{eff}, D_{dis}, f, $\langle \mathbf{v}_g \rangle^g$, and δ are, respectively, the effective diffusion coefficient, a hydrodynamic dispersion coefficient, a rarefaction function, the average velocity of the gas phase, and the Kronecker symbol. In the case of the matrix surrounding the fibers (matrix I), δ is equal to 0 while ε_m is not equal to zero, because the matrix protects the fibers. Otherwise, δ is equal to 1. Fick's law can be derived from the Boltzmann equation. In isotropic porous media, the volume-averaged Fick's law keeps the same form in all regimes (continuum to Knudsen), but the effective diffusion coefficient writes as [21]

$$D_{\text{eff}} = \frac{\varepsilon}{\eta} D_{\text{ref}} \qquad (20)$$

where D_{ref} is a reference diffusivity, corresponding to the longitudinal diffusivity into a capillary of diameter d_p. According to Bosanquet's relation, the reference diffusivity is

$$\frac{1}{D_{\text{ref}}} = \frac{1}{D_B} + \frac{1}{D_K} = \frac{1}{1/3\bar{v}\bar{\lambda}} + \frac{1}{1/3\bar{v}d_p} \qquad (21)$$

where D_B and D_K are, respectively, the bulk and the Knudsen diffusivities, and $\bar{v}$ is the mean velocity of the molecules (molecular agitation). The tortuosity η, a geometric factor that characterizes the difference between a straight capillary and the actual tortuous medium as far as molecule trajectories are concerned, must be derived numerically for the material of interest (see Appendix A).

In the continuum regime, the volume-averaging theory shows that the closure of Eq. (7) gives Eq. (19), where D_{dis} is the hydrodynamic dispersion coefficient. According to this theory, the dispersion can be neglected for Péclet numbers smaller than unity [7]. In porous media, the Péclet number is defined as

$$Pe = \frac{\langle \mathbf{v}_g \rangle^g d_p}{D} \left(\frac{\varepsilon}{1-\varepsilon}\right) \qquad (22)$$

PICA-like material preforms have small pores (50 μm) and a high porosity ($\varepsilon > 0.85$). In the case of Stardust reentry, the average gas velocity is of the order of 1 m/s. Moreover, the bulk diffusion coefficient is high (high temperature and moderate pressure). Hence, the Péclet number is small and the hydrodynamic dispersion is negligible for dense gas flows. The dispersion, driven by gas–gas

collisions, becomes smaller with rarefaction. Therefore, D_{dis} will be neglected in all regimes.

We shall assume that $f = 1$ in Eq. (19) for continuum and slip regimes. This is known to be a correct assumption for dense gases [7]. However, with rarefaction, there are less and less gas–gas collisions; hence, f progressively tends toward zero as the Knudsen number increases [22]. In the Knudsen regime ($Kn > 100$), f is equal to zero [22]. Unfortunately, the value of f is not available in the transition regime for the geometry of interest. The aim of this work is to analyze the ability of oxygen to diffuse inside the porous medium; in this case, it is preferred to overestimate the advection effects in the transition regime to provide a lower bound for oxygen penetration. Hence, we shall consider that $f = 1$ in the transition regime. This is not a strong assumption, because the advection generated by pyrolysis gases is found to be small compared with the oxygen transport by diffusion (see Sec. III).

III. Application to the Oxidation of a Carbon Preform

In this section, the models are applied to the analysis of the oxidation of a carbon preform under air to provide some understanding before addressing complex materials. The section is divided into two subsections. In Sec. III.A, the time-dependent ablation of an isothermal carbon preform is analyzed at the microscopic scale using direct numerical simulation. In Sec. III.B, the macroscopic model equations are solved analytically for steady state to provide an understanding of the numerical simulations and to seek for dimensionless numbers.

A. Microscopic Scale: Direct Numerical Simulation

The studied carbon preform is shown in the first pictures of Figs. 5a and 5b. The computational domain is divided into a white part representing the space between the fibers and a black part representing the fibers. The fibrous material is represented on a Cartesian grid in a cube of 100^3 voxels (3-D pixels). The initial conditions in this case were built by filling the volume using a Monte Carlo algorithm in which fibers with random positions and orientations are positioned in the cube until the porosity reaches the target value of 0.85. To realistically reproduce the material architecture, fibers are nonoverlapping and their direction is azimuthally biased so that they are almost parallel to the top surface (± 15 deg).

The 3-D time-dependent solution to the reaction/diffusion problem described previously is obtained using an efficient numerical simulation code named AMA. The code, developed in a previous work [23], uses Monte Carlo random walk to simulate mass transfer from continuum to Knudsen regimes. AMA is a C ANSI implementation with four main features:

1) A 3-D image (graph) containing several phases (fluid and solid in the present case) is described by the discrete cubic voxels method on a Cartesian grid.

2) The moving fluid/solid interfaces [Eq. (1)] are determined by a simplified marching-cube approximation.

3) Mass transfer by diffusion is simulated by a random walk using Maxwell–Boltzmann distribution for the free path in the Knudsen and transition regimes and using a Brownian motion simulation technique in the continuum and slip regimes. Brownian motion is a grid-free method that efficiently converges when simulating diffusion in a continuous fluid [24].

4) Heterogeneous first-order reaction on the wall [Eq. (3)] is simulated by using a sticking probability. The boundary conditions are Dirichlet on top of the domain (i.e., the oxygen concentration is specified, $C = C_0$), Neumann at the bottom (no oxygen flux), and periodic on the sides. Dirichlet boundary condition is handled using a buffer region in which the concentration of walkers is kept constant.

Two simulations carried out on the carbon preform are shown in Figs. 5a and 5b. The material behavior is found to depend on the ratio of diffusion velocity to the oxidant consumption rate inside the porous medium. When the reaction process is fast compared with mass transfer, the oxidant is mostly consumed at the surface and

cannot diffuse into the porous medium; in this case, ablation is a surface phenomenon (Fig. 5b). In the converse case, for slow oxidant consumption rate, the oxidant diffuses between the fibers and its concentration becomes homogeneous in the porous medium (Fig. 5a). The ablation, in this case, occurs in volume (Fig. 5a). The simulation of Fig. 5a has been carried out for Stardust peak heating conditions ($T = 3360$ K and $P = 0.26$ atm). These simulations show that at peak heating, the oxidation of a carbon preform leads to ablation in volume. This volume ablation obviously weakens the structure of the perform that can undergo spallation under shear stress. Note that the diffusion coefficient is proportional to $T^{1.5}$ [17], whereas the reaction coefficient depends exponentially on temperature [Eq. (4)]. Therefore, at lower temperatures, the oxygen penetrates deeper into the structure. The only way to reach a surface recession regime from the conditions of Fig. 5a is to increase the pressure. An increase in pressure reduces the diffusion coefficient, which is inversely proportional to pressure [17]. A parametric variation has shown that to reach a surface ablation regime, we need to increase the pressure to $P = 10$ atm. These are the conditions of the numerical simulation that give the results shown in Fig. 5b. These numerical experiments are interesting because they enable an intuitive understanding through visualization of the evolution of the material. At this point, an analytical study should be performed to provide a comprehensive understanding [i.e., the relevant dimensionless number(s) for the reaction-diffusion competition].

B. Macroscopic Scale: Analytical Study

This subsection is divided into two parts. In the first part, the reaction-diffusion competition is analyzed in steady state in the absence of pyrolysis gas blowing. In the second part, blowing effects are included in the model, and the model is applied to the analysis of oxygen penetration in a carbon preform for the conditions encountered during the entry trajectory of Stardust.

1. Analytical Analysis Without Blowing Effects

The steady-state concentration of oxygen in a carbon preform is analyzed at the initial time, before ablation has significantly reduced the diameter of the fibers. It is assumed that the fiber preform is oxidized in 1-D at the macroscopic scale. Under these hypotheses, Eq. (19) rewrites as

$$\frac{\partial^2 \langle C(z) \rangle^g}{\partial z^2} - \frac{s_f k_f}{D_{eff}} \langle C(z) \rangle^g = 0 \qquad (23)$$

with the conventions of Fig. 2 (there is no matrix in the present model, however). The thickness of the fiber preform is L. The solution to this ordinary differential equation (ODE) in the domain L with a Dirichlet boundary condition at the wall [$C(z = 0) = C_0$] at $z = 0$ and a Neumann condition at the bottom ($d\langle C \rangle^g / dz = 0$) at $z = L$ is

$$\langle C(z) \rangle^g = C_0 \frac{\cosh(\Phi(z/L - 1))}{\cosh \Phi} \qquad (24)$$

where

$$\Phi = \frac{L}{\sqrt{D_{eff}/s_f k_f}} \qquad (25)$$

is the Thiele number. The penetration of oxygen inside the porous medium is then a function of the Thiele number, as shown in Fig. 6. When the Thiele number is small (diffusion is much faster than reaction), the oxidant concentration inside the porous medium is homogeneous and equal to C_0. Ablation is a volume phenomenon (Fig. 5a) in this case. In the converse case (high Thiele number), diffusion is not fast enough to transport the oxidant inside the porous medium; only the top of the sample ablates. Ablation is a surface phenomenon (Fig. 5b) in this case.

In the design of a TPS, knowledge of the effective reactivity k_{eff} of the material can guide the choice of the material; k_{eff} is defined as the
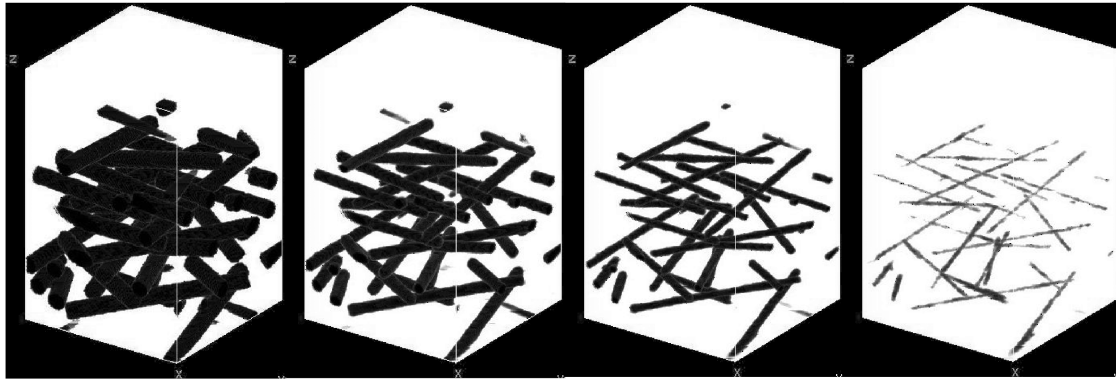
a) Reaction regime : volume ablation *(T=3360 k, p= 0.26 atm, fiber diameter = 10µm, D/k = 2 mm)*
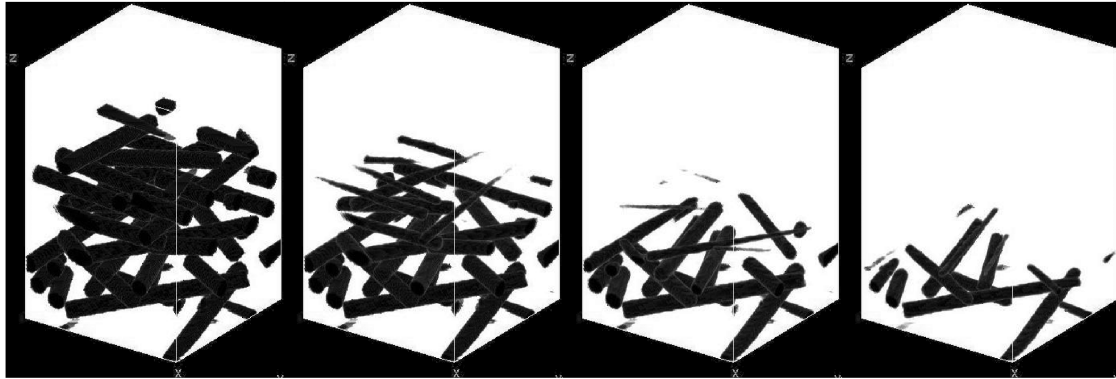
b) Diffusion regime : surface ablation *(T=3360 k, p= 10 atm, fiber diameter = 10µm, D/k = 50 µm)*

Fig. 5   Direct numerical simulation of the ablation of a carbon preform.

reactivity of a homogeneous, dense, and smooth material that would produce the same ablation rate as the porous medium:

$$J_{\text{eff}} = k_{\text{eff}} C_0 = \int_{z=0}^{L} k_f s_f C(z) \, \mathrm{d}z = k_f \int_{z=0}^{L} s_f C(z) \, \mathrm{d}z \qquad (26)$$

The surface of the effective material is placed at abscissa $z = 0$. In this subsection, the material is assumed to be at constant temperature; hence, k_f is constant. Equation (26) shows that k_{eff} is a function of the concentration field inside the porous medium. Hence, k_{eff} is not intrinsic, it is a function of the Thiele number. The use of k_{eff} may then be confusing, because the reactivity is generally seen as an intrinsic property. Instead, the notion of ERSA associated with an intrinsic reactivity k_f may be used. The ratio of the ERSA to the surface area of the effective material, or geometric surface area (GSA), is given by

$$\gamma_{\text{ERSA}} = \frac{\text{ERSA}}{\text{GSA}} = \frac{k_{\text{eff}}}{k_f} = \int_{z=0}^{L} s_f \frac{C(z)}{C_0} \, \mathrm{d}z = sL \frac{\tanh \phi}{\phi} + (1 - \varepsilon)$$

$$(27)$$

where $J_{\text{eff}} = \gamma_{\text{ERSA}} C_0 k_f$. It is interesting to notice that the integral term in Eq. (27) is the surface integral of the specific surface s_f weighted by the local concentration. This provides a physical meaning to the notion of ERSA. To illustrate this, the ERSA coefficient γ_{ERSA} has been plotted in Fig. 7 as a function of the effective diffusion coefficient for the kind of carbon preform represented in the first image of Fig. 5a. For a given intrinsic reactivity, the ERSA coefficient features two limit cases as a function of the diffusion coefficient: surface ablation for low-diffusion
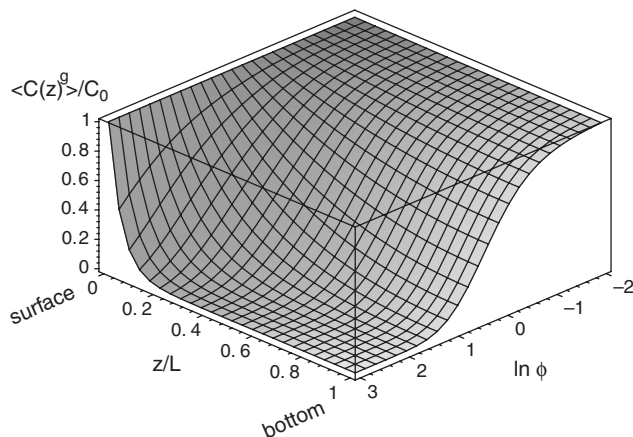

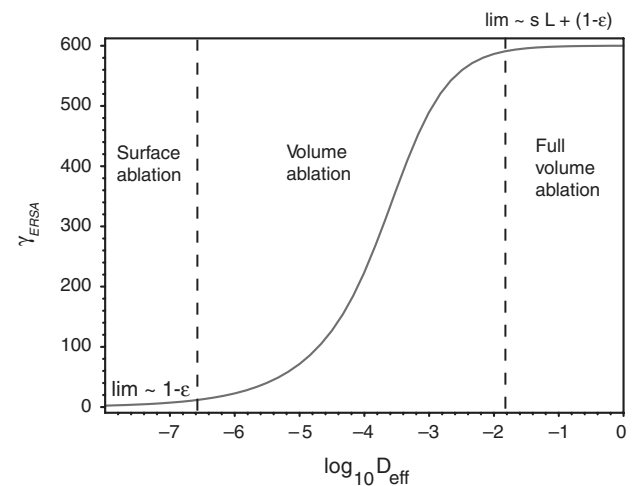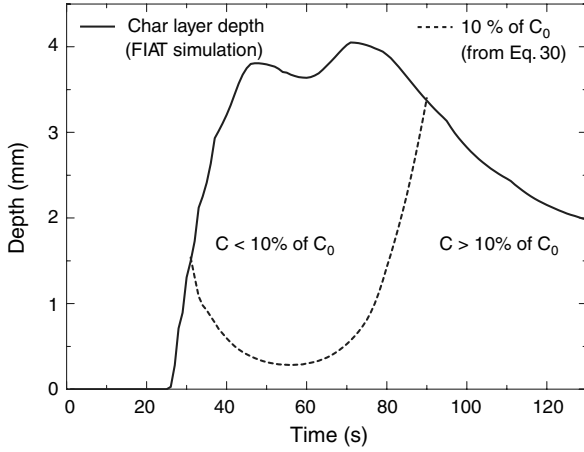**Fig. 6   Oxidant concentration inside the porous medium as a function of Thiele number.**

Fig. 7   Value of the effective reactive surface-area coefficient γ_{ERSA} as a function of the effective diffusion coefficient for $k_f = 1$ m/s, $s = 6 \times 10^5$ m^{-1}, and $L = 1$ cm.

Fig. 8 Estimation of the penetration of oxygen in a fibrous carbon preform of thickness equal to the char-layer depth of the Stardust TPS as a function of time for Stardust reentry conditions at the stagnation point ($t = 0$ is the entry-interface time).

coefficients (i.e., small Thiele numbers) and full volume ablation for high-diffusion coefficients (i.e., large Thiele numbers). In the limit cases, the material behavior is no longer a function of the diffusion coefficient. The plot of Fig. 7 illustrates the fact that the ERSA coefficient may become very large and should be accounted for in finite rate chemistry ablation models. For Stardust peak heating conditions at the stagnation point, the effective diffusion coefficient of molecular oxygen in air in the carbon preform is estimated to be around 3×10^{-3} m/s, leading to a potentially large ERSA coefficient, depending on the value of L.

2. Analytical Analysis Including Blowing Effects

The model presented in the previous section is upgraded to account for blowing effects but is still applied to a carbon preform. This step provides insight before solving the PDE system of the generalized model on a PICA-like material using a numerical method.

Accounting for blowing effects, Eq. (23) rewrites as

$$\frac{\partial^2 \langle C \rangle^g}{\partial z^2} + \frac{1}{L_C} \frac{\partial \langle C \rangle^g}{\partial z} - \frac{1}{L_R^2} \langle C \rangle^g = 0 \qquad (28)$$

where

$$L_C = \frac{D_{\text{eff}}}{\varepsilon \langle v_g \rangle^g} \quad \text{and} \quad L_R = \sqrt{\frac{D_{\text{eff}}}{s_f k_f}} \qquad (29)$$

The solution to this quadratic ODE in a semi-infinite domain, with a Dirichlet boundary condition $[C(z = 0) = C_0]$ at $z = 0$, is

$$\langle C \rangle^g = C_0 \exp\left[-\frac{z}{L_C} \left(1 + \sqrt{1/4 + \left(\frac{L_C}{L_R}\right)^2} \right) \right] \qquad (30)$$

The analytical solution [Eq. (30)] shows that blowing effects are negligible for $L_C > 10 L_R$. For Stardust peak heating conditions at the stagnation point, we estimate that the blowing effects are almost negligible ($L_C = 6.5 L_R$) compared with the oxygen diffusion time scale.

In Fig. 8, the char-layer depth of PICA measured from the receded surface, estimated using FIAT, is plotted (solid line) as a function of trajectory time at the stagnation point. From this data, and knowing temperature and pressure at the wall, the contour of oxygen concentration in a carbon preform of equivalent thickness can be estimated using Eq. (30). The ablation rate inside the preform becomes negligible when the local oxygen concentration $\langle C \rangle^g$ becomes lower than 10% of the wall concentration C_0. This 10% concentration location, plotted (dashed line) in Fig. 8, shows that oxygen penetration in a carbon preform would reach a minimum at

peak heating ($t = 51$ s). At peak heating, the size of the ablation zone would be about 0.4 mm, which, at fiber scale, represents approximately 20 fiber layers. This is an indication that during the whole trajectory, a significant volume of the preform would undergo recession in volume and may spallate due to loss of cohesion of the fibers, as observed in Fig. 5a. Therefore, for a PICA-like material without residual matrix or with a matrix surrounding the fibers (material model I), we expect oxygen penetration into the char layer and significant volumetric ablation. This reveals one of the strong points of the tortuous pore-filling matrix of PICA that protects the preform against volume ablation, at least for a while, before being itself ablated.

IV. Application to PICA-Like Materials in Stardust Reentry Conditions

The results of the previous section show that oxygen penetration in a carbon preform or in a PICA-like material without residual matrix would be a design concern for Stardust reentry conditions. This section aims at applying the same multiscale approach to the analysis of PICA-like material behavior in such conditions. In parallel, the approach will be used to try to explain the observations of Stardust postflight analyses at microscopic and macroscopic scales.

A. Microscopic Approach

The simulation of the oxidation of the char layer of a PICA-like material with a carbonized pore-filling phenolic matrix (material model II) carried out using AMA is presented in Fig. 9. The recession is faster for the matrix than for the fibers. This is explained by the following facts:

1) The reactivity of the carbonized matrix is 10 times higher than the reactivity of the fibers.

2) The matrix-to-fiber density ratio is around $1/32$. Progressively, fibers are stripped out and oxidized, leading to their thinning. In steady state, we can distinguish two recession fronts: the first one is delimited by the tip of the fibers (fiber front), and the second one is the matrix front. The material density decreases from the matrix front to the fiber front. We propose to call the layer of material lying between these two fronts the ablation zone (Fig. 1a).

The presented simulation has been carried out for Stardust peak heating conditions at the stagnation point. Interestingly, in steady state, the thickness of the ablation zone in the PICA-like material is equal to the length of oxygen penetration in the carbon preform of the previous section (Fig. 8). This arises from the fact that, in steady state, the matrix front recession is limited by oxygen transfer. Seen from the carbon preform point of view, this is equivalent to the semi-infinite domain boundary condition chosen to integrate Eq. (28) that led to Eq. (30). That is why the same result is found in steady state. However, in the transient regime, the matrix protects the preform.

The model we are using does not account for spallation. The steady-state image of Fig. 9 seems to indicate that this is a wrong assumption. This first multiscale analysis shows that it is important to improve our multiscale model by accounting phenomenologically for spallation. This improvement is needed to develop accurate macroscopic models that account for mass loss in volume.

The computational time required for the microscopic-scale simulation presented in Fig. 9 is about 24 h on a single processor (frequency of 2 GHz). In comparison, the resolution of the same case using the equivalent macroscopic approach (averaged PDE system) takes only 20 s with the same hardware, using for example a finite element PDE solver (see the next section). This justifies the interest of switching to the macroscopic-scale approach for global analysis and design.

B. Macroscopic Model

The macroscopic oxidation model encompassing Eqs. (8), (10–16), and (19–21) may be used in the analysis of the ablation of the char layer during the last 40 s of the trajectory time considered in Fig. 8. This time interval is particularly interesting because oxidation is expected to occur in the whole char layer. Also, FIAT simulations
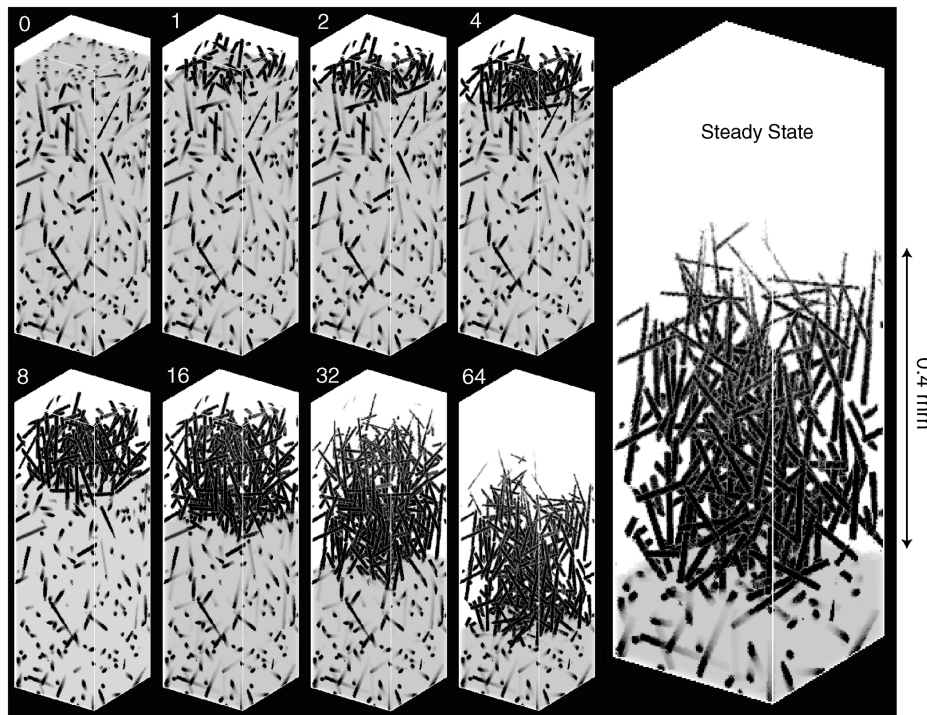
Fig. 9   Three-dimensional microscopic simulation of the oxidation of PICA for Stardust peak heating conditions at the stagnation point ($T = 3360$ K and $P = 0.26$ atm) from a nonablated pyrolyzed state to the steady-state ablation regime.

indicate that the wall temperature is 1380 K at $t = 90$ s, and therefore sublimation is negligible. The thermal gradient in the char layer is predicted to be around 150 K/mm at $t = 90$ s and to decrease with time. At $t = 130$ s, the char-layer temperature is found to be homogeneous and to be around 850 K. For lower temperatures, oxidation can be neglected. In the analysis that we will be presenting, linear interpolations for temperature in time and position are used in the input data of Eqs. (8), (10–16), and (19–21); the pyrolysis gas velocity is around 0.5 m/s. The oxygen concentration at the wall and the pressure, which is assumed constant in the char layer, were obtained from DPLR simulations.

Two kinds of PICA-like materials are considered: one with a matrix surrounding the fibers and the other with a pore-filling matrix. At the initial time, the char-layer density of both materials is assumed to be homogeneous and equal to 230 kg/m³. The average preform density is 180 kg/m³ (preform volume fraction is 0.1 with a density of 1800 kg/m³). Matrix average density is then 50 kg/m³. Accurate determination of the pore-filling matrix properties would require specific experiments. A set of values has been estimated: $\alpha = 7$ and $s_m = 10^6 \varepsilon_m$ m²/m³. The equations are integrated in the char layer on the 90–130 s time interval using a commercial finite element tool (FlexPDE). For both materials, ablation by oxidation is shown to modify the density profile in volume, as represented in Fig. 10. The material with a matrix surrounding the fibers is deeply ablated, because diffusion is fast compared with reaction (low Thiele number). In the other case, closer to PICA, the high-surface-area matrix prevents oxygen diffusion inside the preform and the structure is protected until the matrix is oxidized.

In [4], the measured density of PICA in the char layer is found to be lower than predicted by current pyrolysis and surface ablation models, mainly in the first 0.5 mm. This observation may be explained by volume oxidation. Postflight analyses suggest that the initial density of the char of the PICA version used in Stardust is 210 kg/m³ [4]. Using this initial density value, we can try to fit the measured density drop using the macroscopic model. Figure 11 shows that it is possible to fit flight values using this model. Previously estimated parameters were correct except for the specific surface, which was found to be around $5 \times 10^5 \varepsilon_m$. This analysis confirms that fibers at the surface of the TPS can be very slightly oxidized in the last part of the reentry, whereas the matrix can be totally removed (Fig. 1b, SEM 4). Incidentally, it is interesting to note

that according to the porous medium model, there is no overall surface recession due to oxidation between 90 and 130 s, but a mass loss in volume, mainly due to matrix oxidation.

The macroscopic model developed in this work is shown to be of interest to model volume ablation, which is not captured by current engineering models. A qualitative agreement with experimental observations is obtained. Specific experiments will be useful to accurately determine some critical data (reactivities, specific surface, etc.) and to quantitatively validate the model.
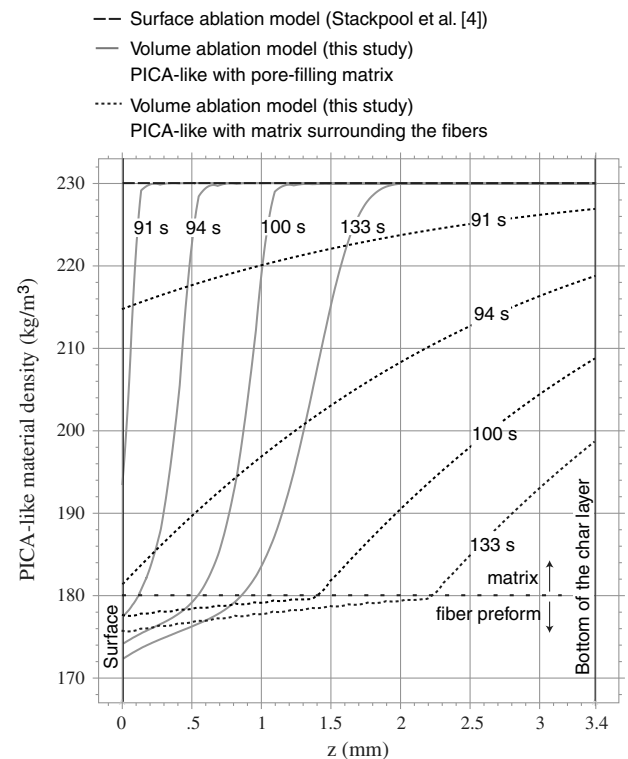

Fig. 10   One-dimensional simulation of the evolution of the density profile of the char layer of two PICA-like materials in the conditions predicted for Stardust reentry between 90 and 130 s.
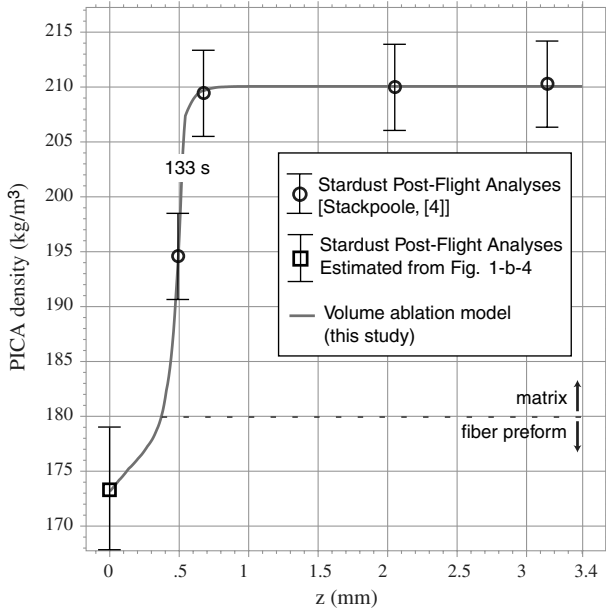
Fig. 11 Fit of measured density using the 1-D macroscopic oxidation model (t = 130 s).

V. Conclusions

A multiscale phenomenological study has been used to analyze and to provide understanding of the ablation of the carbonized char layer of PICA-like materials. The focus has been set on ablation by oxidation under air with the idea that oxygen may diffuse through the pores of the char and ablate the material in depth, leading to the development of an ablation zone.

The starting point of the multiscale modeling strategy is the microscopic scale (i.e., fiber scale). The local surface recessions of the carbon fibers and of the carbonized matrix are individually modeled and coupled to oxygen transport in the porous char. To help in the analysis and to develop a material response model at the macroscopic scale, equations for the response of the char layer have been derived analytically from the microscopic model using volume averaging.

The microscopic and the macroscopic models have been applied to the analysis of the behaviors of a carbon preform and of two PICA-like materials: the first one with a matrix coating the fibers and the second one with a high-surface-area expanded matrix filling the pores of the carbon preform. Three-dimensional numerical simulations have been performed at the microscopic scale and have shown that ablation was controlled by the competition between reaction and diffusion and that ablation could be either a volume or a surface process. The macroscopic model shows that the Thiele number is the key dimensionless number. When the reaction rate is fast compared with mass transfer rate (high Thiele number), the oxidant is mostly consumed at the surface and cannot diffuse through the porous char; in this case, ablation is a surface process (i.e., the thickness of the ablation zone is small compared with fiber diameter). In the converse case (moderate-to-low Thiele number), with the oxidant consumption rate being slow, the oxidant concentration becomes homogeneous inside the porous char and ablation occurs in volume (i.e., the ablation zone encompasses many fiber layers).

The multiscale approach has been applied to Stardust reentry conditions. Oxidation is found to occur in volume at the stagnation point during the whole trajectory and can be a possible explanation to the lower-than-expected density measured for the top layer (0.5 mm) of the char of Stardust TPS (postflight analyses). Microscopic-scale simulations show that volume ablation weakens the structure of the material because the carbonized matrix is deeply ablated, leaving the fibers without protection. The upper layer of the ablation zone is likely to undergo spallation under shear stress exerted at the surface by the surrounding flow. This phenomenon is particularly of concern

in the case of PICA-like material with a matrix coating the fibers. Interestingly, it is found that the pore-filling matrix of the PICA used for the Stardust TPS helps to protect the carbon preform by blocking oxygen diffusion, at least in the transient regime.

As an opening, this study strongly suggests that a spallation model coupled to a physicochemical model is needed to develop accurate macroscopic models that account for mass loss in volume. This implies the necessity of first developing a complete physicochemical volume-ablation model that accounts for sublimation and finite rate chemistry in the gas phase. This model should then be coupled to boundary-layer phenomena (transfer and chemistry) and to the material response model (pyrolysis and heat transfer). Finally, it will be possible to couple this model to a spallation model.

Appendix A: Computation of Effective Diffusion Coefficients by Direct Numerical Simulation

To apply the porous medium model to the analysis of actual problems, knowledge of the effective diffusion coefficient inside the fibrous preform is necessary. Random-walk simulations are used to compute the effective diffusion coefficient in Knudsen and transition regimes. The fibrous preform of PICA-like materials, modeled in Fig. A1, is orthotropic; the diffusion coefficients in the x–y plane and in the z direction are expected to be different. Effective Knudsen, transition, and bulk diffusion coefficients in a given direction j are obtained through a computer simulation using the mean square displacement of a particle (walker) in this direction, $\langle \xi_j^2 \rangle$, after adequately large values of travel time τ of a large population of random walkers introduced randomly in the unit cell of the porous medium. The diffusion coefficient in direction j is then obtained using the following relation [25]:

$$D_{ej} = \frac{\langle \xi_j^2 \rangle}{2\tau} \tag{A1}$$

The effective diffusivity inside the porous medium may be assessed for any combination of mean velocity and mean free path $(\bar{v}, \bar{\lambda})$. However, Eqs. (20) and (21) show that the only data that cannot be determined analytically is the tortuosity. The tortuosity is a function of $\bar{\lambda}$ and the architecture of the porous medium. As a consequence, it is convenient to assess the tortuosity as a function of Knudsen number (Fig. A2). The simulation tool presented in the second section (AMA) is used again. To assure convergence, the simulations have been performed using 10,000 walkers for a path
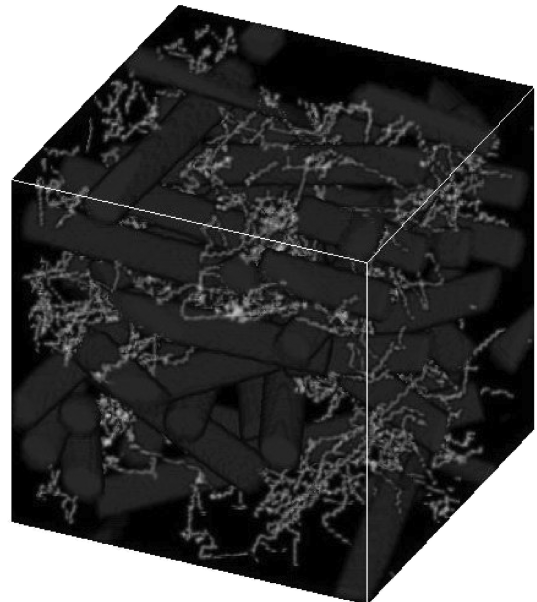

Fig. A1 Path of a random walker (for which the mean free path is 5 μm) inside the porous medium of the study.
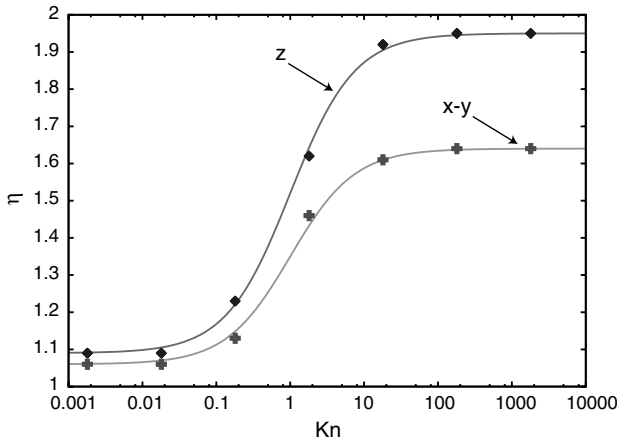
Fig. A2 Tortuosity of the random fibrous medium as a function of Knudsen number for z and x–y directions; DNS (points) and analytical approximations (curves).

1000 times larger than the elementary cell side. The numerical procedure has been validated for a square array of parallel cylinders by comparing the simulation results with analytical results [26] in the bulk diffusion regime and with numerical results in the transition and Knudsen regimes [21,27]. Tomadakis and Sotirchos [21] also studied random fiber structures, but these architectures were isotopic and with overlapping fibers, and so they are not comparable with the anisotropic and nonoverlapping fiber structure of this study. The extension of Bosanquet's relation to ordinary porous media by defining a bulk tortuosity η_B and a Knudsen tortuosity η_K has been shown to provide a good interpolation of numerical data for random fibrous structures [21]. Under this extension, the effective tortuosity writes as

$$\eta = \frac{\eta_B + \eta_K Kn}{1 + Kn} \qquad (A2)$$

The curves of Fig. A2 have been plotted using this approximation. A correct interpolation is obtained again for nonoverlapping fibers. Relation (A2) can then be used in the analytical ablation model.

In the case of PICA-like materials with a pore-filling matrix, the matrix may be modeled independently as a porous medium in which the tortuosity is very high, because the size of the pores is very small compared with the mean free path. The following exponential law is proposed as a first approach:

$$\eta_m = \exp(\alpha \cdot \varepsilon_m) \qquad (A3)$$

where α is a constant to be assessed. Determining α by direct numerical simulation would be feasible if the porous structure of the matrix were known. Unfortunately, this is not available yet. Another method to determine α is inverse analysis. This approach consists of fitting macroscopic experimental results using variation on this parameter (see Sec. IV).

Acknowledgments

References

[1] Tran, H. K., Johnson, C. E., Rasky, D. J., Hui, F. C. L., Hsu, M.-T., Chen, T., Chen, Y. K., Paragas, D., and Kobayashi, L., "Phenolic Impregnated Carbon Ablators (PICA) as Thermal Protection Systems for Discovery Missions," NASA, TM 110440, 1997.

[2] Moyer, C. B., and Rindal, R. A., "An Analysis of the Coupled Chemically Reacting Boundary Layer and the Charring Ablator," NASA CR-1061, 1968.

[3] Milos, F. S., and Chen, Y.-K., "Two-Dimensional Ablation, Thermal Response, and Sizing Program for Pyrolyzing Ablators," AIAA Paper 2008-1223, Jan. 2008.

[4] Stackpoole, M., Sepka, S., Cozmuta, I., and Kontinos, D., "Post-Flight Evaluation of Stardust Sample Return Capsule Forebody Heat-Shield Material," AIAA Paper 2008-1202, Jan. 2008.

[5] Chen, Y.-K., and Milos, F. S., "Navier–Stokes Solutions with Finite Rate Ablation for Planetary Mission Earth Reentries," *Journal of Spacecraft and Rockets*, Vol. 42, No. 6, 2005, pp. 961–970.
doi:10.2514/1.12248

[6] Lachaud, J., Aspa, Y., and Vignoles, G. L., "Analytical Modeling of the Steady State Ablation of a 3D C/C Composite," *International Journal of Heat and Mass Transfer*, Vol. 51, Nos. 9–10, 2008, pp. 2618–2627.
doi:10.1016/j.ijheatmasstransfer.2008.01.008

[7] Whitaker, S., "The Method of Volume Averaging," *Theory and Application of Transport in Porous Media*, edited by J. Bear, Vol. 13, Kluwer Academic, Dordrecht, The Netherlands, 1999, p. 219.

[8] Trumble, K. A., Cozmuta, I., Sepka, S., and Jenniskens, P., "Post-Flight Aerothermal Analysis of the Stardust Sample Return Capsule," AIAA Paper 2008-1201, Jan. 2008.

[9] Wright, M., Candler, G., and Bose, D., "Data-Parallel Line Relaxation Method for the Navier–Stokes Equations," *AIAA Journal*, Vol. 36, No. 9, 1998, pp. 1603–1609.
doi:10.2514/2.586

[10] Desai, P., Qualls, G., and Levit, C., "Stardust Entry Reconstruction," AIAA Paper 2008-1198, Jan. 2008.

[11] Levit, C., "Reconstruction and Verification of the Stardust SRC Re-Entry Trajectory," AIAA Paper 2008-1199, Jan. 2008.

[12] Chen, Y.-K., and Milos, F. S., "Fully Implicit Ablation and Thermal Analysis Program (FIAT)," *Fourth International Conference on Composites Engineering (ICCE/4)*, edited by D. Hui, International Community for Composites Engineering and College of Engineering, New Orleans, LA, 1997, pp. 661–662.

[13] Katardjiev, I. V., Carter, G., Nobes, M. J., Berg, S., and Blom, H.-O., "Three-Dimensional Simulation of Surface Evolution During Growth and Erosion," *Journal of Vacuum Science and Technology A (Vacuum, Surfaces, and Films)*, Vol. 12, No. 1, 1994, pp. 61–68.
doi:10.1116/1.578859

[14] Park, C., *Nonequilibrium Hypersonic Aerothermodynamics*, Wiley, New York, 1990.

[15] Lachaud, J., Bertrand, N., Vignoles, G. L., Bourget, G., Rebillat, F., Weisbecker, P., "A Theoretical/Experimental Approach to the Intrinsic Oxidation Reactivities of C/C Composites And of Their Components," *Carbon*, Vol. 45, 2007, pp. 2768–2776.
doi:10.1016/j.carbon.2007.09.034

[16] Drawin, S., Bacos, M. P., Dorvaux, J. M., and Lavigne, O., "Oxidation Model for Carbon-Carbon Composites," 4th International Aerospace Planes Conference, Orlando, FL, AIAA Paper 92-210, 1992.

[17] Reid, R. C., Prausnitz, J. M., and Poling, B. E., *The Properties of Gases and Liquids*, 4th ed., McGraw-Hill, New York, 1987, p. 688.

[18] Bird, G. A., *Molecular Gas Dynamics and the Direct Simulation of Gas Flow*, Oxford Science, Oxford, 1994.

[19] Boyd, I., "Direct Simulation Monte Carlo for Atmospheric Entry," *Course on Hypersonic Entry and Cruise Vehicles*, von Karman Inst. for Fluid Dynamics, Rhode-St.-Genese, Belgium, 2008.

[20] Anderson, J. D., *Hypersonic and High Temperature Gas Dynamics*, McGraw–Hill, New York, 1989.

[21] Tomadakis, M. M., and Sotirchos, S. V., "Ordinary and Transition Regime Diffusion in Random Fiber Structures," *AIChE Journal*, Vol. 39, No. 3, 1993, pp. 397–412.
doi:10.1002/aic.690390304

[22] Kast, W., and Hohenthanner, C.-R., "Mass Transfer Within the Gas-Phase of Porous Media," *International Journal of Heat and Mass Transfer*, Vol. 43, No. 5, March 2000, pp. 807–823.
doi:10.1016/S0017-9310(99)00158-1

[23] Lachaud, J., and Vignoles, G., "A Brownian Motion Technique to Simulate Gasification and Its Application to C/C Composite Ablation," *Computational Materials Science*, Vol. 44, No. 4, Feb. 2009, pp. 1034–1041.
doi:10.1016/j.commatsci.2008.07.015

[24] Plapp, M., and Karma, A., "Multiscale Finite Difference-Diffusion-Monte-Carlo Method for Simulating Dendritic Solidification," *Journal of Computational Physics*, Vol. 165, No. 2, 2000, pp. 592–619.
doi:10.1006/jcph.2000.6634

[25] Einstein, A., *Investigations on the Theory of Brownian Movement*,

edited by R. Furth, Dover, New York, 1956.

[26] Perrins, W. T., McKenzie, D. R., and McPhedran, R. C., "Transport Properties of Regular Arrays of Cylinders," *Proceedings of the Royal Society of London A*, Vol. 369, No. 1737, 1979, pp. 207–225. doi:10.1098/rspa.1979.0160

[27] Vignoles, G. L., Coindreau, O., Ahmadi, A., and Bernard, D., "Assessment of Geometrical and Transport Properties of a Fibrous C/C Composite Preform as Digitized by X-Ray Computerized Micro-tomography. Part 2: Heat And Gas Transport Properties," *Journal of Materials Research*, Vol. 22, No. 6, 2007, pp. 1537–1550. doi:10.1557/jmr.2007.0216

M. Wright
Guest Editor